ADVANCES IN ELECTRONICS AND ELECTRON PHYSICS, VOL. 81

Application of the Integral Equation Method to the Analysis of Electrostatic Potentials and Electron Trajectories

G. MARTINEZ AND M. SANCHO

Departamento de Física Aplicada III
Fac. de Físicas, Universidad Complutense
Madrid, Spain

I. Introduction

The numerical methods for the analysis of electric and magnetic fields have been an area of continuous interest in the last decades. With the advent of high speed computers, a variety of efficient techniques have been developed that allow us to obtain the solution of almost any desired electromagnetic field configuration.

For the electrostatic case, the problem is reduced to getting the solution of the Poisson equation $\nabla^2\phi = -\rho/\varepsilon$ over a region R, subject to boundary conditions, usually of Dirichlet type. General approaches to the numerical solution of this equation are finite difference schemes, with or without variational formulations and integral equation methods. Any of these approximate methods can convert the differential equation into a linear algebraic

* Portions of this article and Figs. 14, 15, and 16 appear in a previous article by the authors (Reference 28), published and copyrighted by Elsevier Science Publishers (Physical Sciences & Engineering Div.), and are reproduced with their permission.

ISBN 0-12-014681-9

system. Relaxation techniques and random walk simulations have frequently been used to solve the algebraic equations, but nowadays the easy access to efficient matrix inversion algorithms incorporated in subroutine libraries makes direct methods preferable. Relative merits of the different approaches have been the subject of extensive discussion (Steele, 1987). In general, the election of the most convenient method for solving a potential problem is very much dependent on the following factors:

i) Facilities of computing memory size and time available. Difference methods, which use a mesh defined over the *volume*, are much more memory and time consuming than integral equations, which set node points only over the domain *surface*.

ii) The shape and symmetry of the region of interest. Curved contours do not fit well to mesh points defined in finite difference schemes. If the problem has rotational or translational symmetry, a two-dimensional formulation is possible and requires a simpler treatment. Another aspect to consider is if the field problem domain extends in all directions to infinity, i.e., if we have an exterior problem. In that case an integral formulation that considers only points around the boundary is better suited.

iii) Medium linearity and uniformity. Difference formulae can be used even when nonlinear and nonuniform media are present. Integral equations are only valid for linear media but can be applied to the frequent case of boundaries over which the permittivity varies discontinuously.

The integral formulation gives directly charge densities induced on the conductor surfaces or the potential and electric field at any desired point. Therefore, it has been frequently used for the calculation of capacitance coefficients of a set of conductors or the computation of trajectories in the electrostatic focusing of ion beams, with or without space charge effects (Renau *et al.*, 1982; Martinez and Sancho, 1983a; Munro, 1987).

II. Integral Equations for Conductors and Dielectrics

In order to derive the integral equations for electrostatic problems, it is convenient to start with an analysis of the discontinuities occurring in the integrals associated with the potentials produced by single or double layers of charge. These integrals are of the form

$$I(\mathbf{r}) = \int_S \sigma(\mathbf{r}') \frac{1}{|\mathbf{r} - \mathbf{r}'|} ds' \tag{1}$$

$$J(\mathbf{r}) = \int_S \tau(\mathbf{r}') \frac{\partial}{\partial n'} \left(\frac{1}{|\mathbf{r} - \mathbf{r}'|} \right) ds'. \tag{2}$$

The integral $I(\mathbf{r})$ is a continuous function, but its normal derivative approaches different limits from each side of the surface. These limits are (Kellogg, 1967)

$$\left(\frac{\partial I}{\partial n}\right)_+ = \left(\frac{\partial I}{\partial n}\right)_0 - 2\pi\sigma(\mathbf{r}) \tag{3}$$

$$\left(\frac{\partial I}{\partial n}\right)_- = \left(\frac{\partial I}{\partial n}\right)_0 + 2\pi\sigma(\mathbf{r}), \tag{4}$$

where n is the outwardly directed normal at $\mathbf{r}$, $(\partial I/\partial n)_+$, $(\partial I/\partial n)_-$ are the limits of the integral from the outer and inner side, and $(\partial I/\partial n)_0$ is the integral at the surface (taken as its Cauchy's principal value).

Similarly, the potential produced by a double layer $J(\mathbf{r})$ is discontinuous, the limits from either side being related to the value J_0 at the surface by the equations

$$J_+ = J_0 + 2\pi\tau(\mathbf{r}) \tag{5}$$

$$J_- = J_0 - 2\pi\tau(\mathbf{r}). \tag{6}$$

Now, we will deduce an integral equation for the electrostatic potential in a geometry including conducting and dielectric media. First of all, if we have a set of charged conductors, the potential that they produce is

$$\phi(\mathbf{r}) = \frac{1}{4\pi\varepsilon_0} \int_{S_C} \frac{\sigma(\mathbf{r}')}{|\mathbf{r} - \mathbf{r}'|} ds', \tag{7}$$

where $\sigma(\mathbf{r}')$ is the charge density and S_C represents the surface of all the conductors.

When Eq. (7) particularizes to points lying on the surface of any conductor where the potential is constant and known, it constitutes a Fredholm integral equation of first class. Its solution gives $\sigma(\mathbf{r}')$ and then the potential at any point, using Eq. (7) again.

We consider now a system of conducting and homogeneous dielectric bodies, as shown in Fig. 1. We will treat the dielectric interfaces as transitions from one dielectric body with permittivity ε_i to the vacuum and then to another dielectric with ε_j or to a conductor and assume that the transition layer is vanishingly thin.

The potential at any point inside a dielectric volume is produced by all sources present in the space. In our case these are basically surface charges on the conductors with density $\sigma(\mathbf{r}')$ and dipole distributions over the polarized dielectrics, described by the polarization vector $\mathbf{P}(\mathbf{r}')$. In addition, other

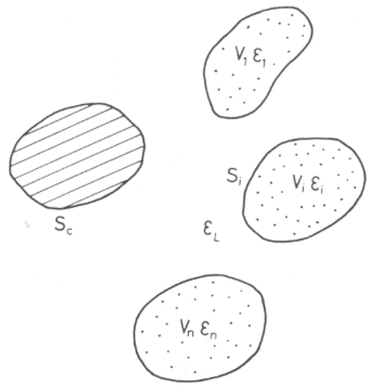

FIG. 1. Schematic drawing of a set of conducting and dielectric bodies.

possible sources, such as space charges with volume density $\rho(\mathbf{r}')$, can be considered. Then we have

$$\phi(\mathbf{r}) = \frac{1}{4\pi\varepsilon_0}\int_V \frac{\rho(\mathbf{r}')}{R}dv' + \frac{1}{4\pi\varepsilon_0}\int_{S_C}\frac{\sigma(\mathbf{r}')}{R}ds' + \sum_{J=1}^{N}\frac{1}{4\pi\varepsilon_0}\int_{V_J}\mathbf{P}(\mathbf{r}')\nabla'\left(\frac{1}{R}\right)dv', \tag{8}$$

where $R = |\mathbf{r} - \mathbf{r}'|$, V_J represents the volume of the dielectric J, V is the total volume, and S_C is the surface of all conductors. If we express $\mathbf{P}(\mathbf{r}') = \varepsilon_0(k-1)\mathbf{E}(\mathbf{r}')$, Eq. (8) becomes

$$\phi(\mathbf{r}) = \frac{1}{4\pi\varepsilon_0}\int_V \frac{\rho(\mathbf{r}')}{R}dv' + \frac{1}{4\pi\varepsilon_0}\int_{S_C}\frac{\sigma(\mathbf{r}')}{R}ds' - \frac{1}{4\pi}\sum_J(k_J-1)\int_{V_J}\nabla'\phi(\mathbf{r}')\nabla'\left(\frac{1}{R}\right)dv'. \tag{9}$$

Using partial integration and replacing the integrals of the divergence by surface integrals, we obtain

$$\phi(\mathbf{r}) = \frac{1}{4\pi\varepsilon_0}\int_V \frac{\rho(\mathbf{r}')}{R}dv' + \frac{1}{4\pi\varepsilon_0}\int_{S_C}\frac{\sigma(\mathbf{r}')}{R}ds' - \frac{1}{4\pi}\sum_J(k_J-1)\left(\int_{S_J}\phi(\mathbf{r}')\nabla'\left(\frac{1}{R}\right)ds' - \int_{V_J}\nabla^2\left(\frac{1}{R}\right)\phi(\mathbf{r}')dv'\right). \tag{10}$$

With the substitution $\nabla^2(1/R) = -4\pi\delta(\mathbf{r}-\mathbf{r}')$, and if the point $\mathbf{r}$ belongs to the dielectric volume V_I, Eq. (10) becomes

$$\phi(\mathbf{r}) = \frac{1}{4\pi\varepsilon_0 k_I}\int_V \frac{\rho(\mathbf{r}')}{R}dv' + \frac{1}{4\pi\varepsilon_0 k_I}\int_{S_C}\frac{\sigma(\mathbf{r}')}{R}ds' - \frac{1}{4\pi k_I}\sum_J(k_J-1)\int_{S_J}\phi(\mathbf{r}')\frac{\partial}{\partial n'}\left(\frac{1}{R}\right)ds', \qquad \mathbf{r}\in V_I. \tag{11}$$

To obtain an integral equation we apply this expression to a point very close to the surface S_I, an interface between the dielectrics I and L. Because of the continuity of the potential, and using Eqs. (5) and (6) to write the terms corresponding to this interface as integrals from the surface, we get

$$\phi(\mathbf{r}) = \frac{1}{2\pi\varepsilon_0(k_I+k_L)}\int_V \frac{\rho(\mathbf{r}')}{R}dv' + \frac{1}{2\pi\varepsilon_0(k_I+k_L)}\int_{S_C}\frac{\sigma(\mathbf{r}')}{R}ds' - \frac{1}{2\pi(k_I+k_L)}\sum_J(k_J-1)\int_{S_J}\phi(\mathbf{r}')\frac{\partial}{\partial n'}\left(\frac{1}{R}\right)ds' \tag{12}$$

for the field point on a dielectric interface; k_I and k_L are the relative permittivities of the media I and L, which are in contact along the interface.

For points on an interface dielectric-conductor, $\phi(\mathbf{r})$ is constant and the corresponding integral vanishes, so there is no discontinuity and an equation similar to Eq. (11) is obtained,

$$\phi(\mathbf{r}) = \frac{1}{4\pi\varepsilon_0 k_I}\int_V \frac{\rho(\mathbf{r}')}{R}dv' + \frac{1}{4\pi\varepsilon_0 k_I}\int_{S_C}\frac{\sigma(\mathbf{r}')}{R}ds' - \frac{1}{4\pi k_I}\sum_J(k_J-1)\int_{S_J}\phi(\mathbf{r}')\frac{\partial}{\partial n'}\left(\frac{1}{R}\right)ds', \tag{13}$$

where k_I is the electric permittivity of the medium in contact with the conducting surface at $\mathbf{r}$. Potentials at the conductors are known, so Eqs. (12) and (13) are a system of integral equations for the potential along the dielectric interfaces and the charge densities on the conductors. Once these unknowns have been obtained, Eq. (11) gives the potential at any desired point.

An expression for the electric field at $\mathbf{r}\in V_I$ is also readily obtained from the potential given by Eq. (11),

$$\mathbf{E}(\mathbf{r}) = \frac{1}{4\pi\varepsilon_0 k_I}\int_V \frac{\rho(\mathbf{r}')\mathbf{R}}{R^3}dv' + \frac{1}{4\pi\varepsilon_0 k_I}\int_{S_C}\frac{\sigma(\mathbf{r}')\mathbf{R}}{R^3}ds' - \frac{1}{4\pi k_I}\sum_J(k_J-1)\int_{S_J}\phi(\mathbf{r}')\frac{\partial}{\partial n'}\left(\frac{\mathbf{R}}{R^3}\right)ds', \qquad \mathbf{r}\in V_I, \tag{14}$$

with $\mathbf{R} = \mathbf{r} - \mathbf{r}'$.

III. Numerical Technique

We are interested in solving the set of integral equations by a method that must have two main characteristics: power and flexibility. These criteria will enable the study of a wide variety of problems with the highest efficiency. In what follows, we describe the numerical technique that we have developed to attain this goal.

A. Method of Moments

Harrington (1968) has provided a unified treatment for the numerical solution of linear operator problems. His approach, the method of moments, involves the expansion of the unknown solutions in a series of basis functions and the use of a set of weighting functions to obtain a linear algebraic system. The approach we will follow, closer to the physical picture, is to divide the contours into a set of subsections of nonuniform size chosen in accordance with the expected nonuniformity of the potential and charge density. Thus in the vicinity of metallic corners, the charge density varies approximately as r^{-n}, r being the distance to the corner and n an exponent that depends on the corner angle (Jackson, 1980). A similar reasoning can be applied to the variation of ϕ along a dielectric interface. Thereafter, we divide the surfaces into progressively smaller subareas close to the vertex, so that a constant value of σ or ϕ can be assumed on each of them. Mathematically it is equivalent to the use of pulse functions defined over the corresponding subsection as basis functions in the moment method, but the election of nonuniform subareas has proved to have an accuracy comparable to that of much more complicated versions. A second choice, which further simplifies the computation of the matrix elements, is the use of Dirac delta functions as weighting functions. On the other hand, we also approximate the space charge distribution by a set of discrete volume elements in such a way that ρ can be considered of uniform magnitude inside each of them; this will facilitate the calculation of the constant vector of our system.

According to the previous considerations, let the index j go from 1 to k to account for conducting subareas, from $k+1$ to m for dielectrics ones, and from $m+1$ to n for volume elements. The resulting algebraic system, obtained from Eqs. (12) and (13), is then of the form

$$\phi_i = \sum_{j=1}^{k} A_{ij}\sigma_j + \sum_{j=k+1}^{m} B_{ij}\phi_j + \sum_{j=m+1}^{n} C_{ij}\rho_j, \qquad (i = k+1 \ldots m) \tag{15}$$

$$\phi_i = \text{const.} = \sum_{j=1}^{k} D_{ij}\sigma_j + \sum_{j=k+1}^{m} E_{ij}\phi_j + \sum_{j=m+1}^{n} F_{ij}\rho_j, \qquad (i = 1 \ldots k), \tag{16}$$

corresponding to points on the dielectric and on the conductor surfaces, respectively. The expressions for the coefficients are

$$A_{ij} = \frac{1}{2\pi\varepsilon_0(k_i + k_l)} \int_{S_j} \frac{1}{R_{ij}}\, ds' \tag{17}$$

$$B_{ij} = -\frac{k_j - 1}{2\pi(k_i + k_l)} \int_{S_j} \frac{\partial}{\partial n'}\left(\frac{1}{R_{ij}}\right) ds' \tag{18}$$

$$C_{ij} = \frac{1}{2\pi\varepsilon_0(k_i + k_l)} \int_{V_j} \frac{1}{R_{ij}}\, dv' \tag{19}$$

$$D_{ij} = \frac{1}{4\pi\varepsilon_0 k_i} \int_{S_j} \frac{1}{R_{ij}}\, ds' \tag{20}$$

$$E_{ij} = -\frac{k_j - 1}{4\pi k_i} \int_{S_j} \frac{\partial}{\partial n'}\left(\frac{1}{R_{ij}}\right) ds' \tag{21}$$

$$F_{ij} = \frac{1}{4\pi\varepsilon_0 k_i} \int_{V_j} \frac{1}{R_{ij}}\, dv', \tag{22}$$

with $R_{ij} = |\mathbf{r}_i - \mathbf{r}'_j|$.

Details on analytical evaluations of these coefficients, based on their physical interpretation, are given below.

The resultant matrix equation has no special characteristics, such as sparsity or definiteness, but can be solved by standard techniques. We have used the Crout reduction method (Gerald, 1984). After the determination of $\sigma(\mathbf{r})$ on conducting surfaces and $\phi(\mathbf{r})$ at dielectric interfaces, the potential and field at any point of the space can be calculated from the discrete forms of Eqs. (11) and (14), i.e.,

$$\phi(\mathbf{r}_i) = \sum_{j=1}^{k} D'_{ij}\sigma_j + \sum_{j=k+1}^{m} E'_{ij}\phi_j + \sum_{j=m+1}^{n} F'_{ij}\rho_j, \qquad \mathbf{r}_i \in V_I \tag{23}$$

$$\mathbf{E}(\mathbf{r}_i) = \sum_{j=1}^{k} \mathbf{A}'_{ij}\sigma_j + \sum_{j=k+1}^{m} \mathbf{B}'_{ij}\phi_j + \sum_{j=m+1}^{n} \mathbf{C}'_{ij}\rho_j, \qquad \mathbf{r}_i \in V_I. \tag{24}$$

D'_{ij}, E'_{ij} and F'_{ij} have the same mathematical expressions as D_{ij}, E_{ij} and F_{ij}, and

$$\mathbf{A}'_{ij} = \frac{1}{4\pi k_i \varepsilon_0} \int_{S_j} \frac{\mathbf{R}_{ij}}{R_{ij}^3}\, ds' \tag{25}$$

$$\mathbf{B}'_{ij} = -\frac{k_j - 1}{4\pi k_i} \int_{S_j} \frac{\partial}{\partial n'}\left(\frac{\mathbf{R}_{ij}}{R_{ij}^3}\right) ds' \tag{26}$$

$$\mathbf{C}'_{ij} = \frac{1}{4\pi k_i \varepsilon_0} \int_{V_j} \frac{\mathbf{R}_{ij}}{R_{ij}^3}\, dv', \tag{27}$$

where $\mathbf{R}_{ij} = \mathbf{r}_i - \mathbf{r}'_j$.

B. *Evaluation of the Coefficients*

In calculating these coefficients it is helpful to consider their physical meanings. Thus, those containing the form $\int_{S_j} 1/R_{ij}\,ds'$ or $\int_{V_j} 1/R_{ij}\,dv'$ are proportional to the potential created at point $\mathbf{r}_i$ by a uniform charge of unit amplitude over the subarea S_j or in the volume V_j. Similarly, coefficients with an integral of the form $\int_{S_j} \partial/\partial n'(1/R_{ij})\,ds'$ are proportional to the flux of the electric field created by a unit charge at $\mathbf{r}_i$, across the subarea S_j. On the other hand, $\int_{S_j} \mathbf{R}_{ij}/R_{ij}^3\,ds'$ or $\int_{V_j} \mathbf{R}_{ij}/R_{ij}^3\,dv'$ represent the field produced at $\mathbf{r}_i$ by a unit charge uniformly distributed over S_j or inside V_j, and $\int_{S_j} \partial/\partial n'(\mathbf{R}_{ij}/R_{ij}^3)\,ds'$ is minus the gradient of the flux of the electric field produced by a charge at $\mathbf{r}_i$ across S_j.

In problems with rotational symmetry there are two basic types of subareas into which we can divide any surface: annular and cylindrical. Moreover, for problems including space-charge effects it is convenient to consider cylindrical volume elements. For some configurations, truncated conical subsections would also be adequate, but the calculation of the associated coefficients involve, in general, numerical integrations and these will not be treated in the following. In all cases considered, analytical closed expressions can be deduced for the coefficients. This is an important characteristic of our version of the method of moments because it allows the utilization of a minimum size for the matrix equation in the solution of electrostatic problems.

In what follows, we will give the formulae used in the obtainment of these quantities; they will be classified according to the type of subareas and volume elements previously mentioned. Most of the expressions can be found in advanced electromagnetism textbooks and particularly in Durand (1964), but we have preferred to list them for the sake of completeness.

1. *Coefficients Containing the Form* $\int_{S_j} \dfrac{1}{R_{ij}}\,ds'$

a. Circular Annular Subareas The starting point is the potential at the point (r_i, z_i) due to a disk of radius R_d located at an axial distance z_j and uniformly charged with σ,

$$\phi(r_i, z_i) = \frac{\sigma}{2\pi\varepsilon_0}\left[-\varepsilon(1-\varepsilon')\frac{\pi}{2}z + \frac{R_d^2 - r_i^2}{r_1}K(k) + r_1 E(k) + \frac{z^2(R_d - r_i)}{r_1(R_d + r_i)}\Pi(k, m)\right], \tag{28}$$

where

$$z = z_i - z_j \tag{29a}$$

$$r_1 = [(R_d + r_i)^2 + z^2]^{1/2} \tag{29b}$$

$$k = \frac{2(R_d r_i)^{1/2}}{r_1} \tag{29c}$$

$$m = \frac{2(R_d r_i)^{1/2}}{R_d + r_i}, \tag{29d}$$

and K, E and Π represent the complete elliptic integrals of the first, second and third kind, respectively. The parameters ε and ε' compensate for the discontinuity in Eq. (28) due to the charge layer and have the values

$$\varepsilon = \begin{cases} -1, & z < 0 \\ 0, & z = 0 \\ 1, & z > 0 \end{cases} \qquad \varepsilon' = \begin{cases} -1, & r_i < R_d \\ 0, & r_i = R_d \\ 1, & r_i > R_d. \end{cases} \tag{29e}$$

There are several particular cases in which Eq. (28) reduces to simpler equations,

$$\phi(0, z_i) = \frac{\sigma}{2\varepsilon_0}\left[(R_d^2 + z^2)^{1/2} - |z|\right] \tag{30}$$

$$\phi(R_d, z_i) = \frac{\sigma}{2\pi\varepsilon_0}\left[-\frac{\pi}{2}|z| + r_1 E(k)\right] \tag{31}$$

$$\phi(r_i, 0) = \frac{\sigma}{2\pi\varepsilon_0}\left[(R_d + r_i)E(k) + (R_d - r_i)K(k)\right]. \tag{32}$$

The coefficients we are searching for may now be calculated by superposition of the potential due to a disk of radius equal to the external radius of the annulus, charged with $\sigma = +1$, and that of a disk of radius equal to the internal radius, charged with $\sigma = -1$.

b. Cylindrical Subareas In this geometry the potential created by a semi-infinite cylindrical layer is used. That quantity is expanded in a series of Legendre polynomials and has different expressions depending on the region in which the field point is located (see Fig. 2).

For a point (r_i, z_i) in region I, the potential produced by a cylinder of radius R_c, with its origin at z_j and charged with σ is

$$\phi(r_i, z_i) = -\frac{\sigma R_c}{2\varepsilon_0}\left[\ln(d + z) - \frac{1}{2}\sum_{n=1}^{\infty} \frac{C_{-1/2}^n}{n}\left(\frac{R_c}{d}\right)^{2n} P_{2n-1}(\cos\vartheta)\right]. \tag{33}$$

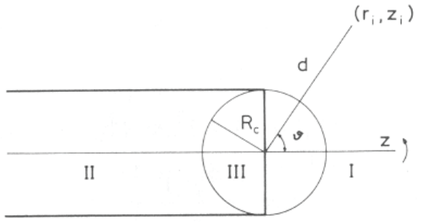

FIG. 2. Different regions for the calculation of the potential due to a semi-infinite cylindrical layer.

For region II, we have

$$\phi(r_i, z_i) = -\frac{\sigma R_c}{2\varepsilon_0}\left[2\ln R_c - \ln(d - z) - \frac{1}{2}\sum_{n=1}^{\infty}\frac{C^n_{-1/2}}{n}\left(\frac{R_c}{d}\right)^{2n} P_{2n-1}(\cos\vartheta)\right]. \tag{34}$$

Finally, for points in region III the potential is

$$\phi(r_i, z_i) = -\frac{\sigma R_c}{2\varepsilon_0}\left[\ln R_c + \sum_{n=0}^{\infty}\frac{C^n_{-1/2}}{2n+1}\left(\frac{d}{R_c}\right)^{2n+1} P_{2n+1}(\cos\vartheta)\right], \tag{35}$$

where $P_n(\cos\vartheta)$ are the Legendre polynomials,

$$C^n_{-1/2} = (-1)^n \frac{1 \times 3 \times \ldots \times (2n-1),}{2 \times 4 \times \ldots \times 2n}, \qquad C^0_{-1/2} = 1, \tag{36}$$

and $d = [r_i^2 + (z_i - z_j)^2]^{1/2}$.

The coefficient associated with a strip of width $z_{j1} - z_{j2}$ is obtained by superposing the potentials created by two semi-infinite cylinders of radius R_c, charged with densities $+1$ and -1, shifted along the axis and with their origins at z_{j1} and z_{j2}.

2. *Coefficients Containing the Form* $\int_{V_j} \frac{1}{R_{ij}} dv'$

For this type of coefficient we only have characterized the one corresponding to a finite cylinder uniformly charged with volume density ρ, because any space charge distribution can be approximated by a set of such cylinders. Hence, we start with the determination of the potential created at the point (r_i, z_i) by a semi-infinite cylinder of radius R_c, charged with ρ (see Fig. 3). This value can be obtained by integration, through the radial distance, of the

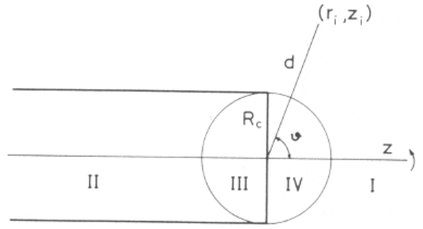

FIG. 3. Different regions for the calculation of the potential created by a semi-infinite cylinder.

potential due to a semi-infinite layer uniformly charged (Eqs. 33 to 35). Depending on the region to which the field point belongs, different expressions are obtained. Thus, for region I we have

$$\phi(r_i, z_i) = -\frac{\rho R_c^2}{4\varepsilon_0}\left[\ln(d + z) - \sum_{n=1}^{\infty}\frac{C^n_{-1/2}}{2n(n+1)}\left(\frac{R_c}{d}\right)^{2n} P_{2n-1}(\cos\vartheta)\right]. \tag{37}$$

For points in region II the integration gives

$$\begin{aligned}\phi(r_i, z_i) &= -\frac{\rho R_c^2}{4\varepsilon_0}\left[\left(\frac{y}{R_c}\right)^2 [\ln(d + z) - 2\ln y + 1] + 2\ln R_c - 1\right. \\ &\quad \left. - \left(1 - \left(\frac{y}{R_c}\right)^2\right)\ln(d - z) - \sum_{n=1}^{\infty}\frac{C^n_{-1/2}}{2n(n+1)}\left(\frac{R_c}{d}\right)^{2n} P_{2n-1}(\cos\vartheta)\right].\end{aligned} \tag{38}$$

When ϑ tends to π, the potential converges to the value

$$\phi(0, z_i) = -\frac{\rho R_c^2}{4\varepsilon_0}\left[\ln\left(\frac{R_c^2}{2d}\right) - 1 + \sum_{n=1}^{\infty}\frac{C^n_{-1/2}}{2n(n+1)}\left(\frac{R_c}{d}\right)^{2n}\right]. \tag{39}$$

For region III we obtain

$$\begin{aligned}\phi(r_i, z_i) &= -\frac{\rho d^2}{4\varepsilon_0}\left[\left(\frac{y}{d}\right)^2 [\ln(d + z) - 2\ln y + 1]\right. \\ &\quad + \left(\frac{R_c}{d}\right)^2 [\ln R_c - 0.5] + \left[\left(\frac{y}{d}\right)^2 - 1\right]\ln(d - z) + \ln d - 0.5 \\ &\quad \left. + \sum_{n=0}^{\infty}\left(\frac{2C^n_{-1/2}}{1 - 4n^2}\left[\left(\frac{d}{R_c}\right)^{2n-1} - 1\right] - \frac{C^{n+1}_{-1/2}}{2(n+1)(n+2)}\right) P_{2n+1}(\cos\vartheta)\right].\end{aligned} \tag{40}$$

For $\vartheta = \pi$, this expression gives

$$\phi(0, z_i) = -\frac{\rho d^2}{4\varepsilon_0}\left[\left(\frac{R_c}{d}\right)^2(\ln R_c - 0.5) - \ln 2 - 0.5 - \sum_{n=0}^{\infty}\left(\frac{2C^n_{-1/2}}{1-4n^2}\left[\left(\frac{d}{R_c}\right)^{2n-1} - 1\right] - \frac{C^{n+1}_{-1/2}}{2(n+1)(n+2)}\right)\right]. \quad (41)$$

Finally, for region IV,

$$\phi(r_i, z_i) = -\frac{\rho d^2}{4\varepsilon_0}\left[\ln(d+z) + \left(\frac{R_c}{d}\right)^2(\ln R_c - 0.5) - \ln d + 0.5 + \sum_{n=0}^{\infty}\left(\frac{2C^n_{-1/2}}{1-4n^2}\left[\left(\frac{d}{R_c}\right)^{2n-1} - 1\right] - \frac{C^{n+1}_{-1/2}}{2(n+1)(n+2)}\right)P_{2n+1}(\cos\vartheta)\right]. \quad (42)$$

In these formulae $y = d\sin\vartheta$, $P_n(\cos\vartheta)$ are the Legendre polynomials, and coefficients $C^n_{-1/2}$ are given in Eq. (36).

The potential due to a finite cylinder is obtained by superposing the potentials created by two semi-infinite cylinders of radius R_c, charged with densities $+1$ and -1 shifted along the axis for a distance equal to the length of the cylinder. Finally, the potential due to a hollow cylinder is given by the appropriate superposition of two cylinders of radii R_1 and R_2 equal to the internal and external radii of the annulus, respectively.

3. *Coefficients Containing the Form* $\int_{S_j}\frac{\partial}{\partial n'}\left(\frac{1}{R_{ij}}\right)ds'$

In this case we are dealing with the calculation of the flux of the electric field of a charge q, at (r_i, z_i), through the area S_j.

a. Circular Annular Subareas We first write the flux of a charge q through a disk of radius R_d; in this equation we take as positive the flux toward the negative z direction,

$$F(S_j) = \frac{q}{4\pi\varepsilon_0}\left[\varepsilon(1-\varepsilon')\pi + \frac{2z}{r_1}[\varepsilon'(1-m^2)^{1/2}\Pi(k,m) - K(k)]\right], \quad (43)$$

where z, k, r_1, m and ε, ε' are given in Eqs. (29a to 29e).

For some particular cases we have

$$F(S_j) = \frac{q}{2\varepsilon_0}\left[\varepsilon - \frac{z}{(R_d^2 + z^2)^{1/2}}\right], \qquad \text{for} \quad \mathbf{r}_i = (0, z_i), \quad (44)$$

$$F(S_j) = q\left(\frac{\varepsilon}{4\varepsilon_0} - \frac{zK(k)}{2\pi\varepsilon_0 r_1}\right), \qquad \text{for} \quad \mathbf{r}_i = (R_d, z_i), \quad (45)$$

$$F(S_j) = 0, \qquad \text{for} \quad \mathbf{r}_i = (r_i, 0). \quad (46)$$

The value we want may be obtained by appropriate superposition of the flux across two disks.

b. Cylindrical Surfaces The flux through a semi-infinite cylindrical layer is related to that of the disk. For example, it is easy to see in Fig. 4 that for a charge q in the region $z = z_i - z_j > 0$, the field lines that enter the circular area of radius R_c are the same as those that give the net outward flux through the cylindrical surface. Let F_d be the value obtained in Eq. (44) and F_c the flux we look for; depending on the relative position of q, F_c is given by

$$F_c = F_d, \qquad \text{for} \quad z > 0 \quad \text{or} \quad z < 0 \quad \text{and} \quad r_i > R_c, \quad (47)$$

$$F_c = F_d + 4\pi q, \qquad \text{for} \quad z < 0 \quad \text{and} \quad r_i < R_c. \quad (48)$$

There are also some particular expressions; thus in the plane $z = 0$ the flux is

$$F_c = \begin{cases} 0, & r_i > R_c \\ \pi q, & r_i = R_c \\ 2\pi q, & r_i < R_c, \end{cases} \quad (49)$$

and for $r_i = R_c$

$$F_c = \begin{cases} F_d, & z > 0 \\ F_d + \pi q, & z < 0. \end{cases} \quad (50)$$

As in the previous calculations, the flux across the cylindrical layer is computed by superposing the contributions of two semi-infinite cylinders conveniently shifted along the axis.

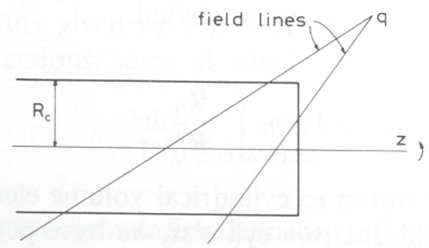

FIG. 4. Diagram for the calculation of the flux through a semi-infinite cylindrical layer.

4. *Coefficients Containing the form* $\int_{S_j} \frac{\mathbf{R}_{ij}}{R_{ij}^3} ds'$.

a. Circular Annular Subareas The components of the field at (r_i, z_i), due to a disk of radius R_d charged with σ at z_j, are

$$E_r(r_i, z_i) = \frac{\sigma}{2\pi\varepsilon_0} \frac{r_1}{r_i} \left[\left(1 - \frac{k^2}{2}\right) K(k) - E(k) \right] \tag{51}$$

$$E_z(r_i, z_i) = \frac{\sigma}{4\pi\varepsilon_0} \left[\varepsilon(1 - \varepsilon')\pi + \frac{2z}{r_1} \left[\varepsilon'(1 - m^2)^{1/2} \Pi(k, m) - K(k) \right] \right], \tag{52}$$

where the variables and parameters have the same meaning as in Eqs. (28) to (30).

Particular simple cases are

$$E_r(r_i, 0) = \frac{\sigma}{2\pi\varepsilon_0} \frac{1}{r_i(r_i + R_d)} [(r_i^2 + R_d^2)K(m) - (r_i + R_d)^2 E(m)] \tag{53}$$

$$E_z(0, z_i) = \frac{\sigma R_d^2}{2\varepsilon_0} \frac{z}{|z|^3} \frac{1}{1 + tg^2\left(\frac{R_d}{|z|}\right)}. \tag{54}$$

The expressions for circular annular subareas are obtained by adequate superposition.

b. Cylindrical Subareas We have now for a semi-infinite cylindrical layer the expressions

$$E_r(r_i, z_i) = \frac{\sigma}{\pi\varepsilon_0} \frac{R_c}{r_i} \left[(1 + \varepsilon')\frac{\pi}{4} - \frac{z}{2r_1} [\varepsilon'(1 - m^2)^{1/2} \Pi(k, m) + K(k)] \right] \tag{55}$$

$$E_z(r_i, z_i) = \frac{\sigma R_c}{\pi\varepsilon_0} \frac{K(k)}{r_1}, \tag{56}$$

with the customary meaning for the symbols used.

The field for a finite cylindrical surface is obtained by superposition of two contributions of this type, adequately shifted.

5. *Coefficients Containing the Form* $\int_{V_j} \frac{\mathbf{R}_{ij}}{R_{ij}^3} dv'$

We restrict our attention to cylindrical volume elements. To obtain the components of the field due to a cylinder, we have performed an approach similar to that used for the coefficients F_{ij}. Thus, for the axial component E_z at the point (r_i, z_i), the elemental contributions of semi-infinite cylindrical

surfaces, uniformly charged, are integrated. We have

$$E_z(r_i, z_i) = \frac{\rho}{\pi\varepsilon_0} \int_0^{R_c} \frac{r' K(k)}{r_1} dr'. \tag{57}$$

As there is no closed analytical expression for Eq. (57), we have developed $K(k)$ in a power series and performed the integration term by term (Byrd and Friedman, 1971). We then write

$$E_z(r_i, z_i) = \frac{\rho}{\varepsilon_0} \left(\sum_{m=0}^{\infty} 2^{2m-1} c_m r_i^m \int_0^{R_c} \frac{r'^{m+1}}{r_1^{2m+1}} dr' \right), \tag{58}$$

where c_m are the coefficients of the expansion for $K(k)$. The integrals appearing in Eq. (58) are reducible to a summation (Gradshteyn and Ryzhik, 1980).

For the radial component, it is easier to use flat disks, uniformly charged, as differential elements and extend the integration between the limits z_1 and z_2 of the cylinder, that is

$$E_r(r_i, z_i) = \frac{\rho}{2\pi\varepsilon_0} \int_{z_1}^{z_2} \frac{r_1}{r_i} \left(\left(1 - \frac{k^2}{2}\right) K(k) - E(k) \right) dz'. \tag{59}$$

We also expand $E(k)$ in series. Then after some algebraic manipulations, Eq. (59) becomes

$$E_r(r_i, z_i) = \frac{\rho}{\varepsilon_0} \left(\sum_{m=2}^{\infty} 2^{2(m-1)} r_i^{m-1} R_c^m (c_m - d_m - 0.5 c_{m-1}) \int_{z_1}^{z_2} \frac{1}{r_1^{2m-1}} dz' \right), \tag{60}$$

where d_m are the coefficients of the series development for $E(k)$. Again, the integrals in Eq. (60) are calculable by means of the appropriate reduction formulae. Furthermore, it is possible to generate each term using calculations previously stored, which allows for a very efficient algorithm.

6. *Coefficients Containing the Form* $\int_{S_j} \frac{\partial}{\partial n'} \left(\frac{\mathbf{R}_{ij}}{R_{ij}^3} \right) ds'$

In this case the components can be obtained by derivation of the corresponding electric flux given by Eqs. (43) to (50). We will not include the rather complex expressions, some of which can be consulted in Algora del Valle *et al.* (1987).

IV. Examples

The integral equation formulation described in Section II can be applied to the study of a great variety of problems in which the potential distribution, for a given set of boundary conditions, is needed. In this section we intend to

illustrate with three representative examples, the way that must be followed for the obtainment of the parameters characterizing the system under analysis. The first one is a bioelectrical problem dealing with transport through ion channels in membranes; its simulation requires the use of two dielectric media as well as polarizing conductors. The second and third examples are related to the Electron Optics area: given a distribution of polarized conductors, their imaging properties are investigated. The last example also shows how space-charge effects can be incorporated into the equations. The particular version of the numerical technique developed here limits the applicability to problems with rotational symmetry; however, this is not a serious restriction as many practical systems can be represented by this type of geometry.

A. Electrostatic Model for Ion Channels

Biological cells are surrounded by a membrane that protects their components from the environment. In most cases, the membrane consists of a lipid bilayer forming a dielectric shield that prevents penetration by ions. It can be shown that the lipid represents a large electrostatic energy barrier (Parsegian, 1969). Of course, metabolites must traverse membranes, and several transport mechanisms have been proposed (Frömter, 1983). One of the most relevant is the transport mediated by fixed channels, where the particle crosses the membrane through a performed permeation path. During the last years considerable experimental, as well as theoretical, work has been done in order to get a deeper insight into that mechanism (Andersen, 1983; Jordan 1986; Jordan *et al.*, 1989).

It is generally agreed that long-range electrostatic forces significantly influence ionic transport through membrane spanning channels. An adequate integral formulation of the problem will allow us the analysis in detail of this type of interaction. A different integral approach has been formulated previously by Jordan (1982), but it was inadequate for the incorporation of exact boundary conditions.

1. *Image Potential*

Figure 5 shows a schematic drawing of a cylindrical channel piercing a membrane of electric permittivity ε_2. The pore and the water are supposed to be characterized by the same permittivity ε_1. An ion of charge q is located at z_0 and induces surface charges along the phase boundaries. Certainly, real channels will not have exact rotational symmetry, but this approximation will permit the use of our numerical technique without introducing too much error.

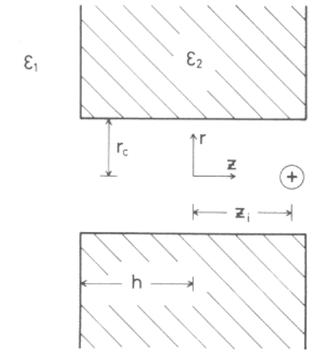

FIG. 5. Cross-sectional diagram of a cylindrical channel spanning a membrane of electric permittivity ε_2. The bulk water and the channel region have the same permittivity ε_1.

According to the formulation given in Section II, the potential at a point lying on the membrane boundary is obtained from Eq. (12). In this case there are not any conducting surfaces and the expression reduces to

$$\phi(\mathbf{r}) = \frac{1}{2\pi\varepsilon_2(\chi+1)}\frac{q}{|\mathbf{r}-z_0\mathbf{k}|} + \frac{\chi-1}{2\pi(\chi+1)}\int_{S_M}\phi\frac{\partial}{\partial n'}\left(\frac{1}{R}\right)ds', \qquad (61)$$

where $\chi = \varepsilon_1/\varepsilon_2$ and the normal n' is taken in the direction outward from the membrane.

For the numerical solution of Eq. (61), we make a division of the phase boundary into n small subareas that have the form of flat circular annuli or cylindrical sections and assume that the induced potential on each of them is constant. Hence, the above expression can be approximated by the set of algebraic equations

$$\phi_i(\mathbf{r}_i) = \frac{1}{2\pi\varepsilon_2(\chi+1)}\frac{q}{|\mathbf{r}_i-z_0\mathbf{k}|} + \sum_{j=1}^{n} B_{ij}\phi_j, \qquad (i=1\ldots n), \qquad (62)$$

$$B_{ij} = \frac{\chi-1}{2\pi(\chi+1)}\int_{S_j}\frac{\partial}{\partial n'}\left(\frac{1}{R_{ij}}\right)ds', \qquad (63)$$

$\mathbf{r}_i$ being the position vector of the midpoint of S_i. The matrix elements B_{ij} are proportional to the flux of the electric field created by a unit charge at $\mathbf{r}_i$ across S_j and can be obtained from Eqs. (43)–(50). After computing the potential distribution along the phase boundary, application of Eq. (11) enables us to find the potential at any point of the aqueous medium. This value is given by

$$\phi(\mathbf{r}) = \frac{1}{4\pi\varepsilon_1}\frac{q}{|\mathbf{r}-z_0\mathbf{k}|} + \frac{\chi-1}{4\pi\chi}\int_{S_M}\phi\frac{\partial}{\partial n'}\left(\frac{1}{R}\right)ds', \qquad (64)$$

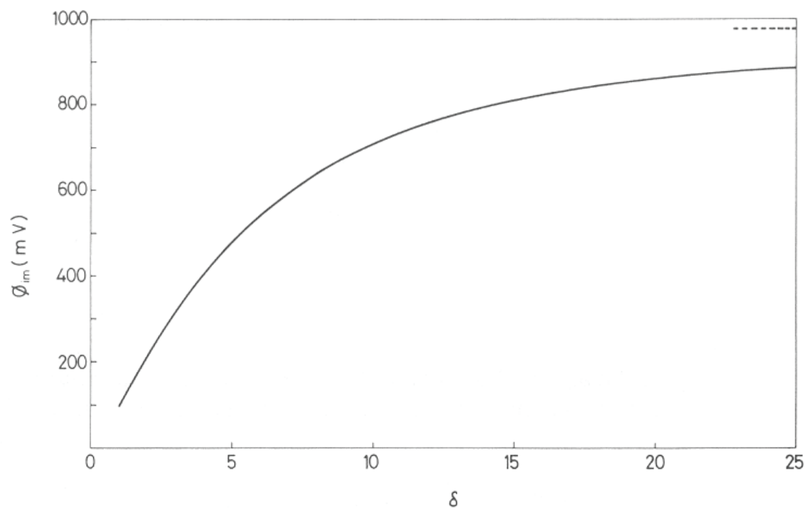

FIG. 6. Image potential ϕ_{im}, for an ion at the center of the channel as a function of the half-width to radius ratio, δ. The asymptotic value (broken line) for an infinite pore is 0.978 volts.

which, expressed in a discrete form and ignoring the contribution of the charge q, may be used to determine the image potential ϕ_{im}, i.e., the potential created by the induced charges at the ion position z_0 along the channel axis. Figure 6 shows this value, for a monovalent cation at $z_0 = 0$ as a function of the half-width to radius ratio, $\delta = h/r_c$. We have chosen $\varepsilon_1 = 80\,\varepsilon_0$ and $\varepsilon_2 = 2\varepsilon_0$, which approximately represents a lipid-water system.

The image potential is positive, as might be expected for $\varepsilon_1/\varepsilon_2 > 1$, and increases with δ. It tends to the asymptotic value 0.978 volts obtained for a pore of infinite length (Parsegian, 1975).

Finally, we must point out that for a Gramicidin-like channel ($\delta = 5$) the potential barrier for passage of a monovalent cation is 0.476 volts, a still significant value. As we will see, this barrier may be altered by the presence of other charge sources such as dipoles along the channel, charges on conductors placed near the membrane, etc.

2. *Polarized Channel*

When a voltage is applied to the pore, Eq. (61) must be modified in order to include the effect of the charges on the electrodes; in addition, there is another expression for points lying on the conducting surfaces S_C, derived from Eq. (13). We assume that the electrodes are flat circular disks, placed at both sides of the channel at a distance $\mp h'$ from the center and polarized with $\pm V_0$.

For simplicity we also take $q = 0$. Then we have

$$\phi(\mathbf{r}) = \frac{\chi - 1}{2\pi(\chi + 1)} \int_{S_M} \phi \frac{\partial}{\partial n'}\left(\frac{1}{R}\right) ds' + \frac{1}{2\pi\varepsilon_2(\chi + 1)} \int_{S_C} \frac{\sigma}{R} ds' \qquad (65)$$

$\mathbf{r} \in$ diel. bound.

$$\phi(\mathbf{r}) = \frac{\chi - 1}{4\pi\chi} \int_{S_M} \phi \frac{\partial}{\partial n'}\left(\frac{1}{R}\right) ds' + \frac{1}{4\pi\varepsilon_1} \int_{S_C} \frac{\sigma}{R} ds' \qquad (66)$$

$\mathbf{r} \in$ cond. surf.

$\phi(\mathbf{r})$, being in Eq. (66), equal to $\pm V_0$ depending on the position of $\mathbf{r}$.

Applying the same numerical technique as in the previous study we obtain

$$\phi_i = \sum_{j=1}^{n} B_{ij}\phi_j + \sum_{j=n+1}^{m} A_{ij}\sigma_j, \qquad (i = 1 \ldots n), \qquad (67)$$

$$\phi_i = \sum_{j=1}^{n} E_{ij}\phi_j + \sum_{j=n+1}^{m} D_{ij}\sigma_j = \begin{cases} +V_0, z_i = -h' \\ -V_0, z_i = h' \end{cases}, \qquad (i = n+1 \ldots m), \qquad (68)$$

where A_{ij} and D_{ij} are related to the potential that is created at point $\mathbf{r}_i$ by a uniform charge density of unit amplitude over S_j. These coefficients may be computed by means of the corresponding analytical expressions given in Eqs. (28)–(36). When the algebraic system is solved for σ_j and ϕ_j, we are able to determine the potential at any point of interest. Table I shows field at the center of the channel (in units of V_0/δ) and the fractional potential drop across the channel, as functions of the ratio δ. It must be pointed out that these quantities depend on the electrode position, the tabulated ones corresponding to a distance $h' = 6h$. Jordan (1982) has reported values for

TABLE I

ELECTRIC FIELD AT THE CENTER OF THE CHANNEL AND FRACTIONAL POTENTIAL DROP AS FUNCTIONS OF THE RATIO δ

δ	Field at the center (V_0/δ)	Fractional potential drop V/V_0
15.0	0.815	0.792
10.0	0.794	0.772
7.5	0.774	0.752
5.0	0.738	0.716
2.5	0.648	0.625
1.25	0.526	0.499

V/V_0 of 20% greater than that shown in Table I; this is presumably due to the fact that the procedure used by Jordan to include the effect of the applied potential is strictly correct only in the limit of very long, narrow channels and overestimates the field in the pore interior (Jordan, 1989).

3. *Dipolar Effects*

It is known that the kinetics of narrow channels, such as Gramicidin in lipid membranes, is strongly influenced by electrostatic interaction between the ion and the permanent dipoles of the polypeptide. Furthermore, several recent studies have focused on the behavior of analogues of Gramicidin A in which one or more amino acids were replaced by others with side chains of different polarity (Andersen *et al.*, 1987; Daumas *et al.*, 1989).

To simulate this experimental situation, dipolar rings near the pore wall are superposed to the geometry given in Fig. 5. These distributions are characterized by a total moment p and can have radial and axial components and be situated at different positions along the channel lumen.

For the polarized channel, the corresponding integral equations are now

$$\phi(\mathbf{r}) = \frac{\chi - 1}{2\pi(\chi + 1)} \int_{S_M} \phi \frac{\partial}{\partial n'} \left(\frac{1}{R}\right) ds' + \frac{1}{2\pi\varepsilon_2(\chi + 1)} \int_{S_C} \frac{\sigma}{R} ds' + \frac{2\chi}{\chi + 1} \phi_s(\mathbf{r}), \qquad \mathbf{r} \in \text{diel. bound.}, \tag{69}$$

$$\phi(\mathbf{r}) = \frac{\chi - 1}{4\pi\chi} \int_{S_M} \phi \frac{\partial}{\partial n'} \left(\frac{1}{R}\right) ds' + \frac{1}{4\pi\varepsilon_1} \int_{S_C} \frac{\sigma}{R} ds' + \phi_s(\mathbf{r}), \qquad \mathbf{r} \in \text{cond. surf.}, \tag{70}$$

where ϕ_s is a source term containing the contributions of both ion and dipolar rings and represents the potential of these charges in an indefinite medium of permittivity ε_1. The partitioning of the boundaries into small subareas in which the unknowns—charge densities or potentials—are supposed to be constant gives the corresponding set of algebraic equations. Its solution allows us the determination of the potential along the channel axis for several different situations. After a systematic analysis of the computed data we conclude the following remarkable results: 1) Radial components of the dipole moments have very little influence on the potential profiles. This can be interpreted as produced by the cancellation of the dipole field by the "image dipole" induced in the medium ε_2. In the case of axial dipoles, both potentials add. 2) The effect of "negative" dipoles (pointing toward the channel center) is to increase the central barrier, while positive ones facilitate ion passage. 3) Negative dipoles at the center of the channel tend to sharpen the barrier.

Positive dipoles tend to widen it and produce a central potential well. 4) Large positive dipoles can produce noticeable wells at the channel mouth.

Figure 7 illustrates the effect of two axial dipole rings located at $\pm h$ in a gramicidinlike channel; in Fig. 8 the contributions of four dipole rings, two at the ends and two at the center, are superposed.

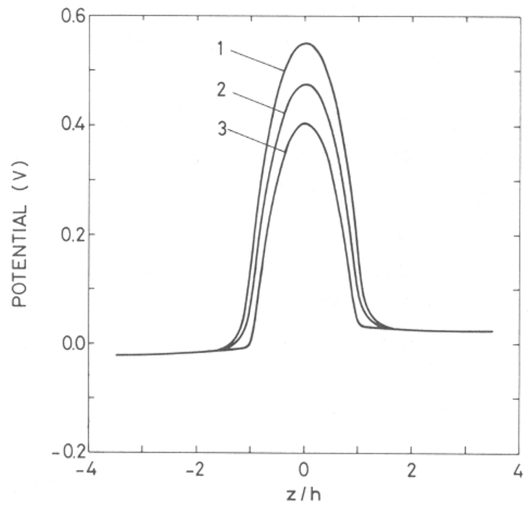

FIG. 7. Potential profile in a channel with one dipole ring at each mouth. ($V_0 = 25$ mV; dipole ring radius $r_d = 0.99\ r_c$; 1: $p = -3$ Debyes; 2: $p = 0$; 3: $p = +3$ Debyes).

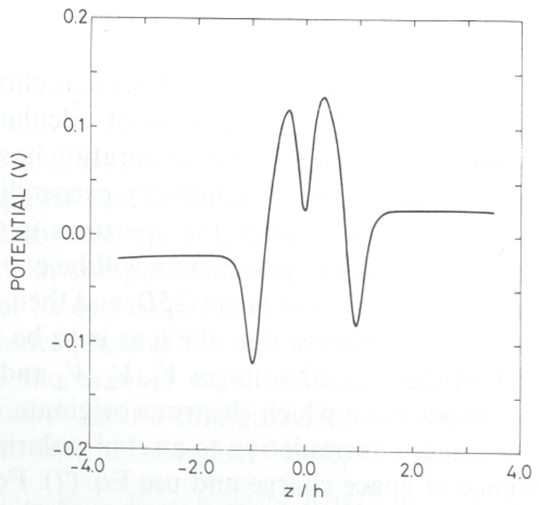

FIG. 8. Potential profile in a channel with four dipole rings: two at the center ($\pm h/12.5$) and one at each mouth. ($V_0 = 25$ mV; dipole ring radius $r_d = 0.99\ r_c$; $p = +8$ Debyes).

It can be seen that axial dipoles pointing toward the pore mouths produce binding positions for the ion and produce potential profiles, such as the one depicted in Fig. 8, which have been proposed to explain the current-voltage characteristics of Gramicidin channels (Levitt, 1986).

B. Four-Aperture Electrostatic Lens

The electrostatic lenses that have been used to focus beams of charged particles have usually consisted of either two or three electrodes, each having the form of either an aperture or a cylinder. The focal properties and aberrations of such lenses have been extensively studied (Grivet, 1972; Harting and Read, 1976; Hawkes, 1987). Although multi-electrode lenses (by which we mean lenses consisting of more than three electrodes) are expected to be better for some purposes and to have properties that are more flexible than those of the simpler two and three electrode lenses, they have been studied less often. In characterizing such lenses Heddle (1971), Kurepa *et al.* (1974) and Chutjian (1979), have made the approximation of treating them as combinations of independent two and three element lenses, which is valid only in a restricted range of geometrical configurations and operating voltages. More recently we have applied our method to the analysis of a four-cylinder lens (Martínez and Sancho, 1983b). As in calculating the axial potential distribution, the technique deals with all the electrodes as a whole; we were able to characterize the operating conditions of practical interest without restrictions. In this paragraph, we present the study of a four-aperture lens following a similar development.

1. *Calculation of Electron-Optical Properties*

Figure 9 shows a cross-sectional diagram of the lens chosen for study. An external equipotential contour, added for the sake of calculation of the optical parameters, is not shown in the figure. The configuration has a horizontal axis of rotational symmetry and a plane of symmetry perpendicular to this axis (the reference plane). The diameter D of the apertures is taken as the fundamental unit of length, and all the parameters will be expressed in units of D. The spacings S between the electrodes are $0.5D$, and their thicknesses T are $0.05D$. It is assumed for convenience that the lens is to be used for focusing electron beams and that the applied voltages V_1, V_2, V_3 and V_4 are measured with respect to the cathode from which electrons originate.

We can apply the integral formulation to a set of polarized conductors in vacuum and in absence of space charge and use Eq. (7). For the purpose of calculation, the electrodes are divided into n subareas that have the form of flat circular annuli or narrow cylindrical sections. Under the assumption that the

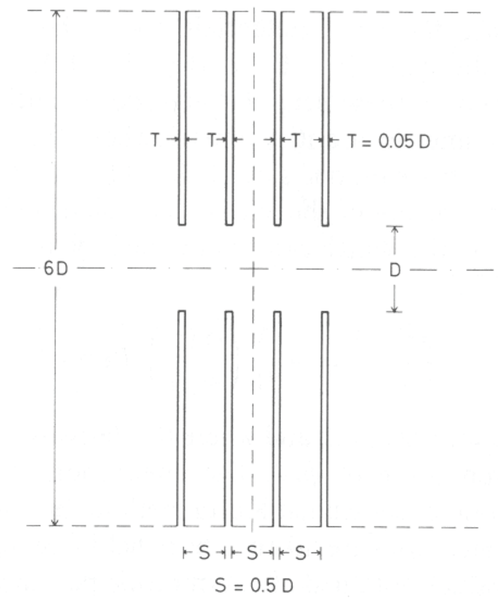

FIG. 9. Cross-sectional diagram of the four-aperture electrostatic lens chosen for study. The fundamental unit of length is the diameter D. The potentials V_1, V_2, V_3 and V_4 are measured with respect to that of the cathode.

charge density σ_j is constant on each subsection of area S_j, the potential at the midpoint $\mathbf{r}_i$ representative of the subsection i can be expressed as

$$\phi_i(\mathbf{r}_i) = \sum_{j=1}^{n} D_{ij}\sigma_j, \qquad (i = 1 \ldots n), \tag{71}$$

with

$$D_{ij} = \frac{1}{4\pi\varepsilon_0}\int_{S_j}\frac{ds'}{R_{ij}}. \tag{72}$$

Having evaluated coefficients D_{ij} by means of the appropriate formulae given in Section III, Eq. (71) can be solved to obtain the charge densities. At this stage we are able to determine the potential at any point within the lens. In particular, we can compute the axial potential, $\phi(z)$, that will allow the characterization of its optical parameters.

Since the reference plane of the lens is a plane of reflection symmetry it is possible to halve the number of subsections required by making use of symmetric and antisymmetric configurations to express $\phi(z)$ in terms of the superposition (Martínez and Sancho, 1983b)

$$\begin{aligned}\phi(z) = {} & 0.25(V_1 - V_2 - V_3 + V_4)\phi_a + 0.25(-V_1 - V_2 + V_3 + V_4)\phi_b \\ & + 0.25(-V_1 + V_2 - V_3 + V_4)\phi_c + 0.25(V_1 + V_2 + V_3 + V_4),\end{aligned} \tag{73}$$

where ϕ_a, ϕ_b, ϕ_c are the axial potentials when the electrode potentials (V_1, V_2, V_3, V_4) have the values $(1, -1, -1, 1)$, $(-1, -1, 1, 1)$, and $(-1, 1, -1, 1)$ respectively. For each of these sets of electrode potentials the charge distribution is either symmetric or antisymmetric about the reference plane, and and hence only subsections on one side of the plane need be considered.

The first order properties of the lens are completely characterized by the focal and midfocal lengths, which can be obtained by integration of the Picht equation (Grivet, 1972)

$$\frac{d^2R(z)}{dz^2} = -\frac{3}{16}\left(\frac{\phi'(z)}{\phi(z)}\right)^2 R(z), \tag{74}$$

where $R(z)$ is the reduced ray path and where the derivative $\phi'(z)$ is determined by numerical differentiation of $\phi(z)$. The integration of Eq. (74) has been carried out by a second order Runge-Kutta method. Because the starting and final points of the trajectories are taken to be in field-free regions on either side of the lens, all the values obtained are asymptotic parameters.

Calculated values of the object focal and midfocal lengths, f_1 and F_1 respectively, and image midfocal length F_2 as functions of V_2/V_1 are given in Fig. 10. The corresponding values of the image focal length f_2 can be deduced from the relationship

$$f_2 = (V_4/V_1)^{1/2} f_1. \tag{75}$$

A comparison with the parameters of the four-cylinder lens (Martínez and Sancho, 1983b) shows a very similar behavior, although the lens studied here is, in general, stronger.

Since the trajectories of the charged particles in the lenses having voltages V_1, V_2, V_3 and V_4 are the time-reversed ones of those in the retarding lenses having $V'_1 = V_4$, $V'_2 = V_3$, $V'_3 = V_2$ and $V'_4 = V_1$, the calculated parameters can be used for obtaining those of the complementary retarding lenses (see Martínez and Sancho (1983b) for the conversion formulae). In this way the range of voltage ratios V_4/V_1 for which the focal lengths have been calculated can be extended to include retarding lenses having V_4/V_1 as low as 0.1.

The spherical aberration can be characterized by the third-order coefficient C_s defined by the relation (Grivet, 1972)

$$\Delta r = MC_s\alpha_0^3, \tag{76}$$

where Δr is the radius of the disk formed in the Gaussian image plane by nonparaxial rays starting from an axial object point with a maximum half angle α_0 and M is the linear magnification for a given object position. Further, it can be shown that C_s is a fourth-order polynomial in $1/M$ (Harting and Read, 1976):

$$C_s(M) = C_{s0} + C_{s1}M^{-1} + C_{s2}M^{-2} + C_{s3}M^{-3} + C_{s4}M^{-4}. \tag{77}$$

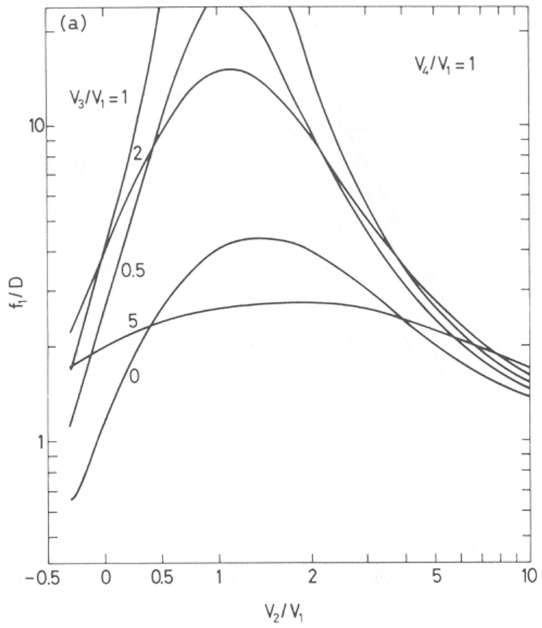

(a)

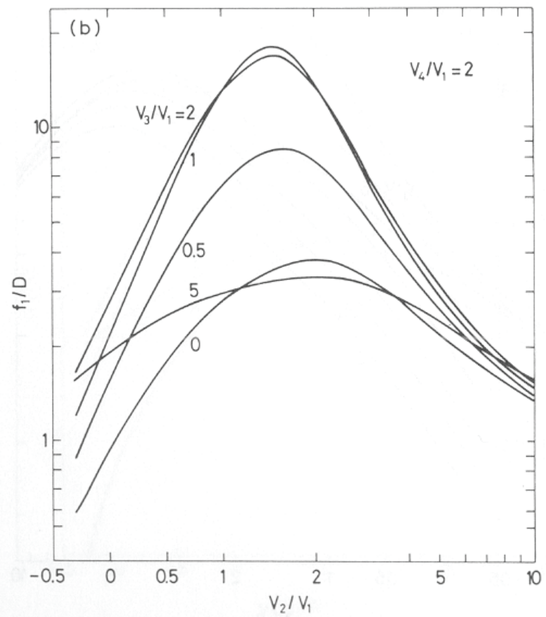

(b)

FIG. 10. The object focal length f_1/D, object midfocal length F_1/D and image midfocal length F_2/D as functions of V_2/V_1. Each plot corresponds to a fixed voltage ratio V_4/V_1, and the numbers on the curves indicate the values of V_3/V_1. Note that the horizontal scale is logarithmic for $V_2/V_1 > 1$ and linear for $V_2/V_1 < 1$.

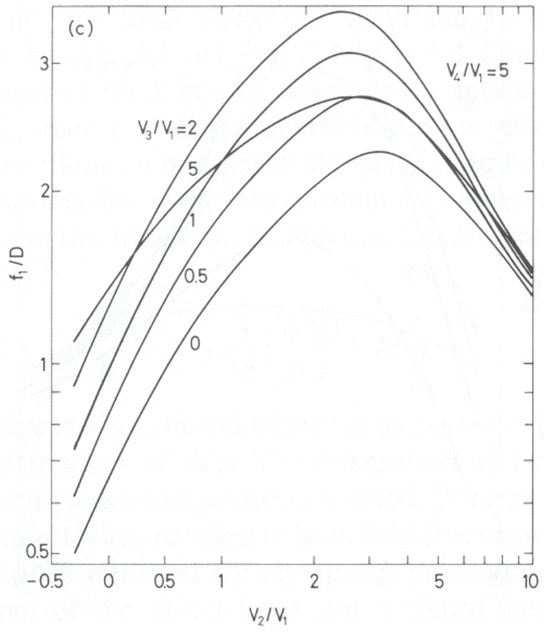

(c)

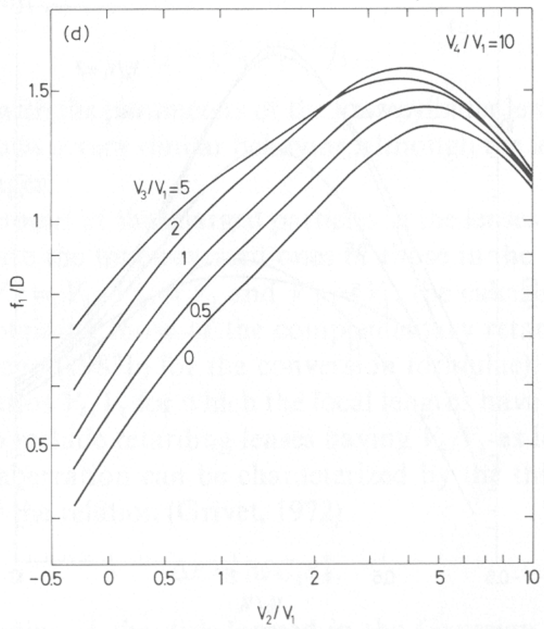

(d)

FIG. 10. (*Cont.*)

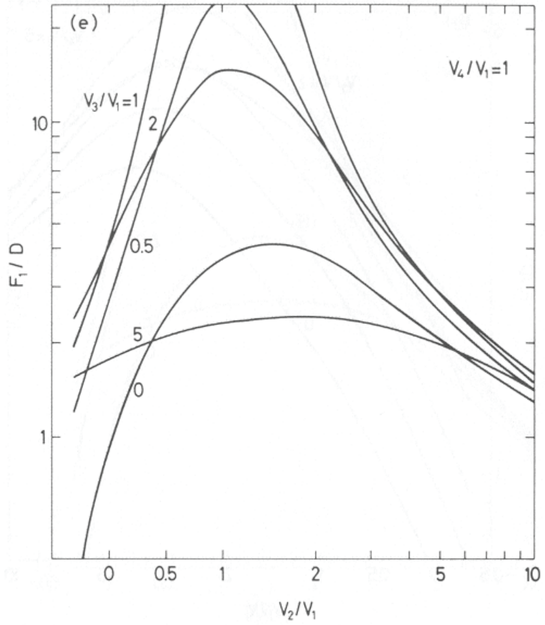

(e)

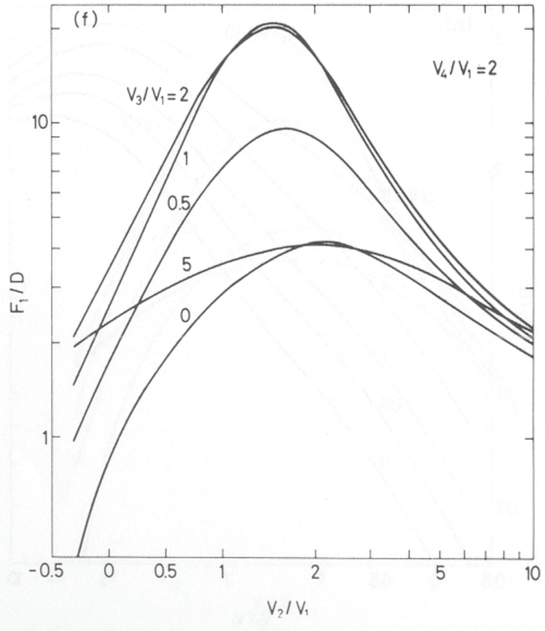

(f)

FIG. 10. (*Cont.*)

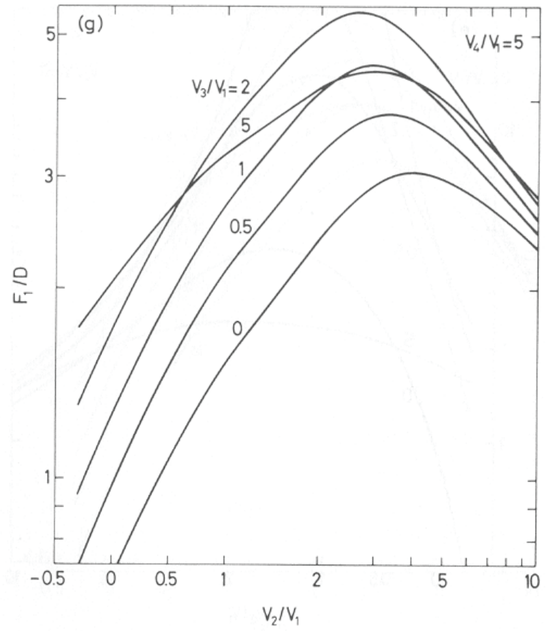

(g)

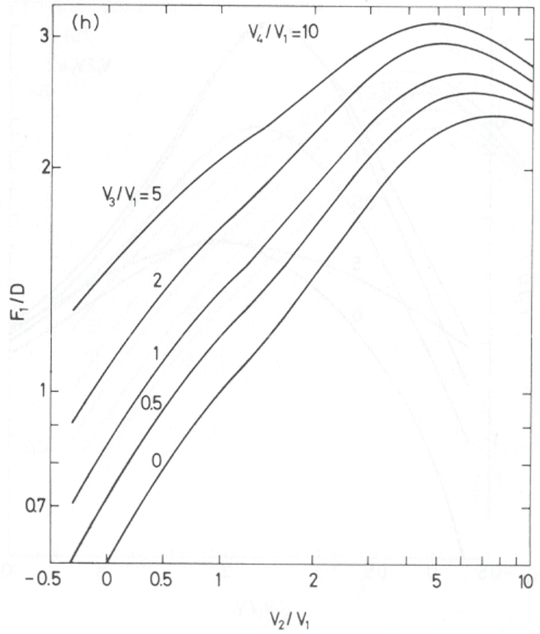

(h)

FIG. 10. (*Cont.*)

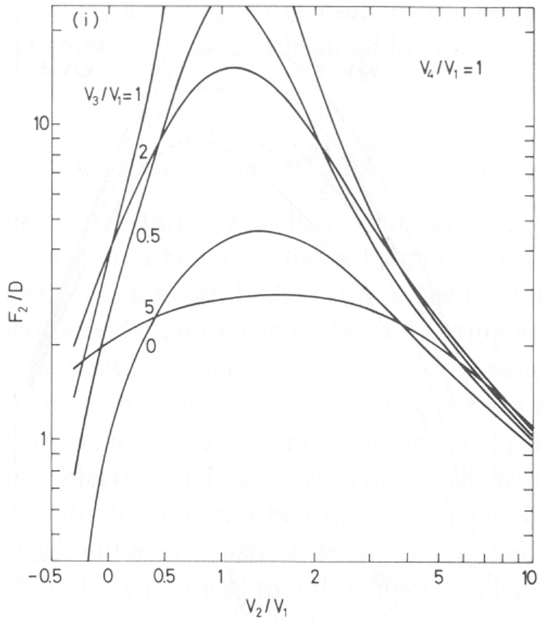

(i)

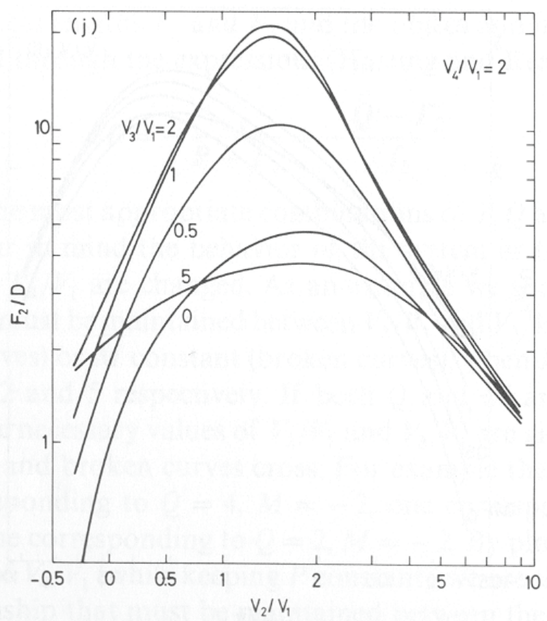

(j)

FIG. 10. (*Cont.*)

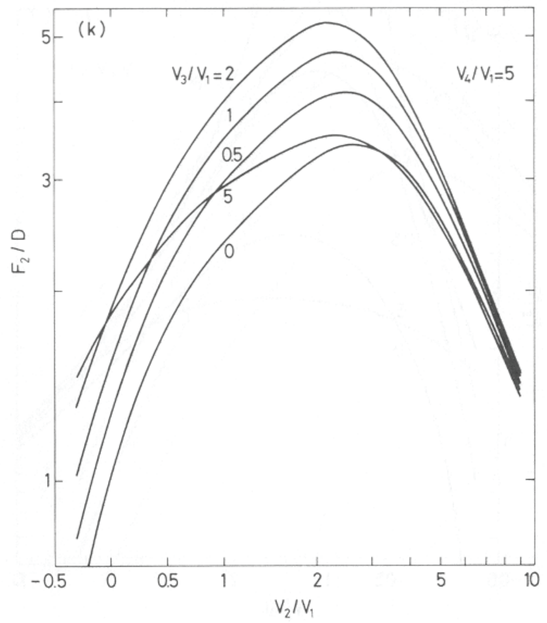

(k)

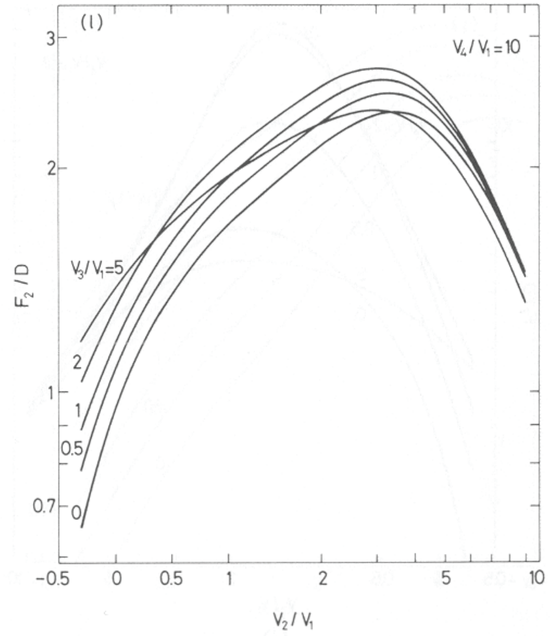

(l)

FIG. 10. (*Cont.*)

Thus, the coefficients C_{si} are frequently used to characterize the spherical aberration. Table II shows the values obtained for the einzel operating mode $V_4/V_1 = 1$.

2. *Energy Scanning at Constant Image Position and Magnification*

Triple-electrode electrostatic lenses have two variable voltage ratios, and so they can be used to focus a beam of charged particles in such a way that the image position is kept constant while the ratio of the final to initial energy of the charges is varied (Heddle and Kurepa, 1970; Harting and Read, 1976). In general, the linear and angular magnifications are not constant. If it is required to keep two parameters constant, such as both the position and magnification of an image, a third variable, voltage ratio, is necessary and the lens must consist of at least four electrodes. In a previous study (Martínez *et al.*, 1983) we showed how a four-cylinder lens can be used to provide an image at a fixed position together with either a constant linear or angular magnification. In what follows, we extend the analysis to a four-aperture lens.

The geometrical configuration of the lens chosen for study is the same as that considered in the preceding subsection, (cf. Fig. 9). For a given set of electrode polarizations, the image linear magnification M, the focal lengths f_1 and f_2, the midfocal lengths F_1 and F_2 and the object and image distances P and Q are related through the expressions (Harting and Read, 1976)

$$M = -\frac{f_1}{P - F_1} = -\frac{Q - F_2}{f_2}. \tag{78}$$

In choosing the most appropriate combinations of P, Q and M values, it is important to bear in mind the behavior of the system as the voltage ratios V_2/V_1, V_3/V_1 and V_4/V_1 are changed. As an example we show in Fig. 11 the relationship that must be maintained between V_2/V_1 and V_3/V_1 to keep either Q constant (full curves) or M constant (broken curves), when P and V_4/V_1 have the fixed values 2 and 5 respectively. If both Q and M are required to be constant, then the necessary values of V_2/V_1 and V_3/V_1 are given by the points at which the full and broken curves cross. For example there are two crossing points corresponding to $Q = 4$, $M = -2$, one corresponding to $Q = 2$, $M = -1$, but none corresponding to $Q = 2$, $M = -2$. By plotting such curves for other values of V_4/V_1 (while keeping P constant), we are thus able to determine the relationship that must be maintained between the electrode potentials for those combinations of P, Q and M for which crossing points exist.

Not all the crossing points represent experimentally suitable modes of the lens. Thus, the crossing points for $Q = 4$, $M = -1$ have low values of both V_2/V_1 and V_3/V_1 and occur in a region where the Q and M curves tend to lie close to each other, which implies that Q and M are sensitive to small changes

TABLE II

SPHERICAL ABERRATION COEFFICIENTS FOR THE MODE $V_4/V_1 = 1$

V_2/V_1	C_{s0}	C_{s1}	C_{s2}	C_{s3}	C_{s4}
			$V_3/V_1 = 0$		
−0.3	6.47 E+1	5.29 E0	1.75 E+1	6.15 E0	1.01 E+1
0.0	9.00 E0	−2.67 E+1	3.68 E+1	−2.67 E+1	9.00 E0
0.5	1.07 E+2	−4.05 E+2	5.84 E+2	−3.81 E+2	9.54 E+1
1.0	4.90 E+2	−1.94 E+3	2.90 E+3	−1.94 E+3	4.90 E+2
2.0	4.65 E+2	−1.80 E+3	2.64 E+3	−1.73 E+3	4.30 E+2
5.0	2.61 E+1	−8.43 E+1	1.08 E+2	−6.62 E+1	1.65 E+1
10.0	4.52 E0	−9.69 E0	1.02 E+1	−6.38 E0	2.39 E0
			$V_3/V_1 = 0.5$		
−0.3	1.25 E+1	−4.57 E+1	6.90 E+1	−4.98 E+1	1.47 E+1
0.0	9.53 E+1	−3.81 E+2	5.83 E+2	−4.05 E+2	1.07 E+2
0.5	3.47 E+3	−1.38 E+4	2.07 E+4	−1.38 E+4	3.47 E+3
1.0	8.38 E+4	−3.35 E+5	5.03 E+5	−3.35 E+5	8.38 E+4
2.0	4.39 E+3	−1.73 E+4	2.57 E+4	−1.69 E+4	4.20 E+3
5.0	2.86 E+1	−1.01 E+2	1.40 E+2	−9.11 E+1	2.36 E+1
10.0	3.80 E0	−9.10 E0	1.08 E+1	−7.54 E0	2.84 E0
			$V_3/V_1 = 2$		
−0.3	8.88 E+1	−3.54 E+2	5.40 E+2	−3.74 E+2	9.88 E+1
0.0	4.28 E+2	−1.72 E+3	2.63 E+3	−1.79 E+3	4.63 E+2
0.5	4.19 E+3	−1.69 E+4	2.56 E+4	−1.73 E+4	4.37 E+3
1.0	9.69 E+3	−3.87 E+4	5.79 E+4	−3.86 E+4	9.65 E+3
2.0	1.27 E+3	−5.03 E+3	7.53 E+3	−5.03 E+3	1.27 E+3
5.0	2.11 E+1	−8.11 E+1	1.25 E+2	−9.08 E+1	2.59 E+1
10.0	2.83 E0	−7.39 E0	1.10 E+1	−9.30 E0	3.77 E0
			$V_3/V_1 = 5$		
−0.3	1.18 E+1	−4.81 E+1	8.21 E+1	−6.73 E+1	2.21 E+1
0.0	1.64 E+1	−6.55 E+1	1.07 E+2	−8.33 E+1	2.58 E+1
0.5	2.33 E+1	−9.02 E+1	1.39 E+2	−9.98 E+1	2.83 E+1
1.0	2.74 E+1	−1.02 E+2	1.49 E+2	−1.01 E+2	2.70 E+1
2.0	2.57 E+1	−9.02 E+1	1.24 E+1	−8.05 E+1	2.10 E+1
5.0	9.34 E0	−2.67 E+1	3.56 E+1	−2.67 E+1	9.34 E0
10.0	3.10 E0	−4.70 E0	7.01 E0	−7.22 E0	4.05 E0

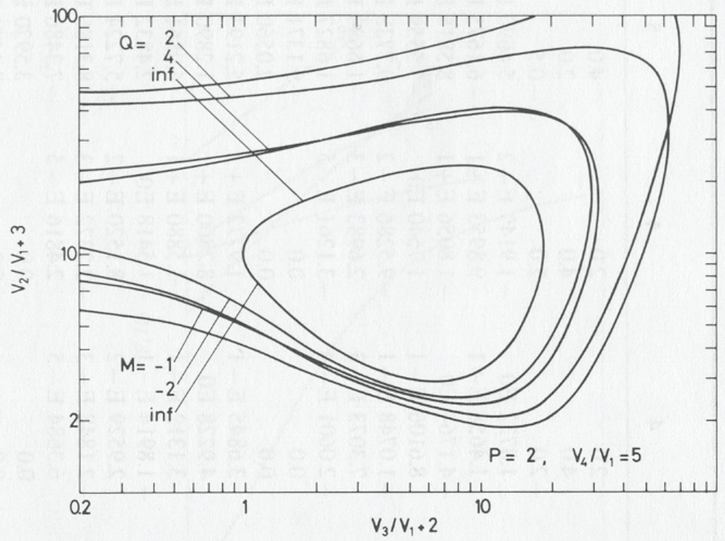

FIG. 11. The relationships that must be maintained between V_2/V_1 and V_3/V_1 when $P = 2$, $V_4/V_1 = 5$, and either Q is constant (full curves) or M is constant (broken curves).

in V_2/V_1 or V_3/V_1. Furthermore, the angle of crossing is very small at these points, and so it is difficult to establish the values of the potentials accurately. This type of working point is therefore excluded from further study. The other crossing points showed are suitable, however. The two that have the highest values of V_3/V_1 give the smallest aberration coefficients, and so we have searched for this type of working point for all the combinations of P, Q and M that we have considered. When this type does not exist or when it exists over only a small range of values of V_4/V_1, we give, instead, data for the crossing points that have the lowest values of V_3/V_1.

For convenience, we present the data on the required voltage ratios in a parametric form for five sets of values of P, Q and M. The voltage ratios of each set are fitted by least squares polynomials giving

$$\frac{V_2}{V_1} = \sum_{n=0}^{N} A_n x^n, \qquad \frac{V_3}{V_1} = \sum_{n=0}^{N} B_n x^n, \tag{79}$$

where $x = V_4/V_1$. For sets 1 and 4, two series of coefficients A_n and B_n are necessary to cover the whole range of the variable x. The values of the fitted coefficients for the five sets are given in Table III.

If one of the focal parameters is known for a constant P, Q and M condition then the remaining three can be obtained from Eq. (78). We therefore show in Fig. 12 the dependence on V_4/V_1 of the object midfocal length F_1 for each of the five sets.

TABLE III

COEFFICIENTS FOR THE POLYNOMIALS GIVING THE VOLTAGE RATIOS FOR EACH OF THE FIVE SETS

Set number	1	1	2	3	Set number	4	4	5
P	2.0	2.0	3.0	4.0	P	2.0	2.0	4.0
Q	2.0	2.0	3.0	4.0	Q	4.0	4.0	2.0
M	−1.0	−1.0	−1.0	−1.0	M	−2.0	−2.0	−0.5
A_0	1.5124 E+1	8.2951 E+2	4.0630 E0	1.9994 E0	A_0	1.8732 E0	−1.9149 E+2	5.4690 E0
A_1	1.5588 E+1	−1.9125 E+2	6.3111 E0	4.8849 E0	A_1	1.4658 E+1	9.8953 E+1	−6.1675 E−1
A_2	−6.5774 E0	1.9825 E+1	−3.4702 E0	−2.1187 E0	A_2	−4.1764 E0	−1.8056 E+1	8.5818 E−1
A_3	1.5366 E0	−1.1499 E0	1.1511 E0	5.3373 E−1	A_3	8.6106 E−1	1.7640 E0	−3.5559 E−1
A_4	−2.0945 E−1	4.1193 E−2	−2.2298 E−1	−4.7132 E−2	A_4	−1.0748 E−1	−9.5286 E−2	9.7738 E−2
A_5	1.7245 E−2	−9.3253 E−4	2.5890 E−2	−3.2342 E−3	A_5	7.3073 E−3	2.6983 E−3	−1.6683 E−2
A_6	−8.4145 E−4	1.3037 E−5	−1.7374 E−3	6.3283 E−4	A_6	−2.0601 E−4	−3.1261 E−5	1.6827 E−3
A_7	2.2353 E−5	−1.0295 E−7	5.9895 E−5	0.0	A_7	0.0	0.0	−9.1371 E−5
A_8	−2.4874 E−7	3.5185 E−10	−7.5304 E−7	0.0	A_8	0.0	0.0	2.0560 E−6
B_0	2.6139 E0	−2.9730 E+2	−1.0513 E0	−1.7107 E0	B_0	3.6845 E−1	1.9772 E+2	5.2193 E0
B_1	2.9010 E+1	9.1443 E+1	1.3352 E+1	1.3221 E+1	B_1	4.9228 E0	−8.2800 E+1	1.2890 E+1
B_2	−7.3381 E0	−9.6829 E0	−6.1856 E0	−9.8541 E0	B_2	3.1312 E−1	1.5880 E+1	−6.9861 E0
B_3	1.3194 E0	5.9230 E−1	2.1819 E0	4.7535 E0	B_3	−1.8914 E−1	−1.5418 E0	2.4832 E0
B_4	−1.5568 E−1	−2.2430 E−2	−5.3443 E−1	−1.3519 E0	B_4	2.9529 E−2	8.1520 E−2	−5.7224 E−1
B_5	1.1747 E−2	5.3707 E−4	8.4363 E−2	2.0143 E−1	B_5	−2.1848 E−3	−2.2372 E−3	8.3186 E−2
B_6	−5.4223 E−4	−7.9403 E−6	−8.1195 E−3	−1.2227 E−2	B_6	6.3684 E−5	2.4816 E−5	−7.3486 E−3
B_7	1.3887 E−5	6.6283 E−8	4.3129 E−4	0.0	B_7	0.0	0.0	3.5920 E−4
B_8	−1.5075 E−7	−2.3945 E−10	−9.6749 E−6	0.0	B_8	0.0	0.0	−7.4444 E−6
V_4/V_1	1.0 − 20.0	20.0 − 52.0	1.0 − 11.2	1.0 − 5.2	V_4/V_1	1.0 − 9.0	9.0 − 20.6	1.0 − 11.5

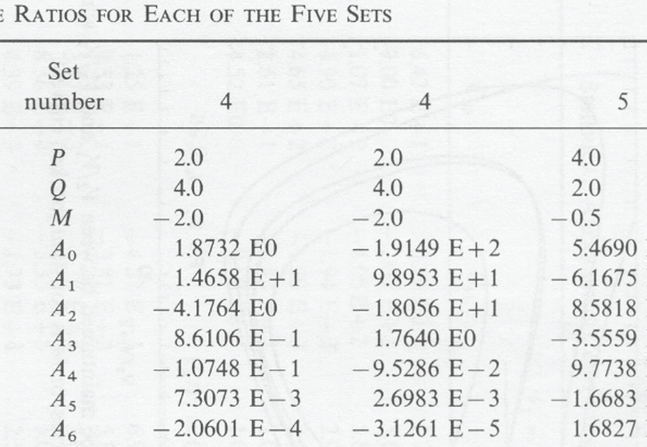

FIG. 12. Variation of F_1/D with V_4/V_1 for the five sets of values P, Q and M specified in Table III.

To characterize the aberrations of the lens we use the third order aberration coefficient C_s defined by Eq. (76). The calculated values of this coefficient are shown in Fig. 13 as a function of V_4/V_1, for each of the sets.

The data given in Table III and Figs. 12 and 13 refer to lenses for which $V_4/V_1 \geq 1$. The corresponding data for retarding lenses can be obtained by comparing the four-aperture lens having voltages V_1, V_2, V_3 and V_4 with the time-reversed analogue having the voltages $V'_1 = V_4$, $V'_2 = V_3$, $V'_3 = V_2$ and $V'_4 = V_1$ respectively. The polynomial expansions given by Eqs. (79) now become

$$\frac{V'_2}{V'_1} = \sum_{n=0}^{N} B_n (x')^{1-n}, \qquad \frac{V'_3}{V'_1} = \sum_{n=0}^{N} A_n (x')^{1-n}, \tag{80}$$

where $x' = V'_4/V'_1$ and the object and image distances and magnification to which they relate are

$$P' = Q, \qquad Q' = P, \qquad M' = M^{-1}. \tag{81}$$

The image midfocal length F'_2 and the spherical aberration coefficients can also be derived from the data in Figs. 12 and 13 and the corresponding conversion formulae (Martínez *et al.*, 1983).

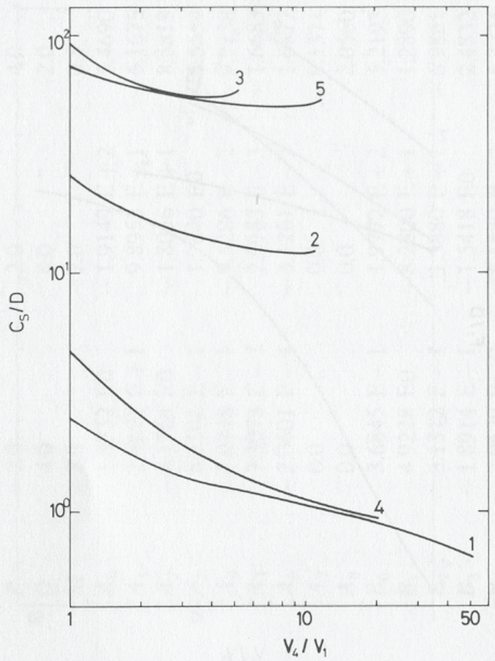

FIG. 13. Variation of C_s/D with V_4/V_1 for the five sets of values, P, Q and M specified in Table III.

The retarding version of the set labeled 4 has the same values of P, Q and M (namely 4, 2 and -0.5 respectively) as the accelerating version of the set labeled 5. Hence the total range of values of V_4/V_1 for which these values of P, Q and M can be maintained extends from 1/20.6 to 11.5, thereby covering more than two decades. Similarly sets 1, 2 and 3, all of which are self-reversing (in the sense that $P = Q = P' = Q'$, $M = M'$), have V_4/V_1 ranges of 1/52 to 52, 1/11.2 to 11.2 and 1/5.2 to 5.2 respectively. These ranges are notably wider than those obtained by the authors for the four-cylinder lens (cf. Martínez *et al.*, 1983). This characteristic together with the fact that the four-aperture lens is comparatively more compact makes it, in general, preferable.

C. *Space-Charge Effects in Lenses*

An interesting aspect of the integral equation method is that it lends itself readily to the solution of electron-optic problems involving space charge. However, as has been noted by Kasper (1987), the direct evaluation of the integral contributions of space charge elements to the potential and the field may represent a great amount of computing time.

Renau *et al.* (1982) have described the general application of the formulation as well as their version of the numerical technique. These authors included space-charge effects using the approximation of linear segments of charge.

Given the error cumulative characteristic of the trajectory computation and the iterative scheme used in this algorithm, it is advantageous to use analytical expressions for the elementary contributions of the space charge. We illustrate this procedure in the following study.

1. *Formulation of the Problem*

Figure 14 shows a cross-sectional diagram of the system under study. We are dealing with a lens proposed by Liebl (1983) for a SIMS equipment. It consists of three plane-apertured electrodes arranged coaxially on the normal of a conducting surface. For the given values of the potentials applied to the electrodes and neglecting space-charge effects, the lens focuses a primary beam of single charged positive ions into a very thin spot and, at the same time, acts as an emission lens for secondary negative ions originating from a surface point.

In a previous work (Martínez *et al.*, 1987), we have obtained some of the trajectories for primary and secondary ions and the results agree qualitatively well with those given by Liebl. Now, we study the case in which the perveance of the primary beam, defined as $P = M^{1/2}IV^{-3/2}$ for singly charged ions of mass number M, is high enough to cause space-charge effects.

Consider the primary beam traveling through the lens. The integral equation for the potential at any point on the electrodes is the same as in Eq. (7) except for a source term that takes into account the contribution of the beam; hence

$$\phi(\mathbf{r}) = \frac{1}{4\pi\varepsilon_0}\left(\int_{S_C} \frac{\sigma(\mathbf{r}')}{R}\,ds' + \int_{V_B} \frac{\rho(\mathbf{r}')}{R}\,dv'\right), \tag{82}$$

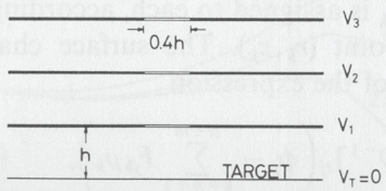

FIG. 14. Cross-sectional diagram of the assembly. Primary ions, generated in a region at potential V_p, enter the lens with energy $e(V_p - V_3)$; secondary ions leave the target with energy $eV_0 \approx 2$–10 eV. The operating voltages are $V_1 = V_2 = 3.55\ V_3$ and $V_p = 4.5\ V_3$.

where $\sigma(\mathbf{r}')$ are the charge densities on the surface S_C of the conductors and $\rho(\mathbf{r}')$ is the beam charge distribution in the volume V_B.

For the numerical solution of Eq. (82) we make, similar to the previous cases, a division of the conductor surfaces into n subareas and the beam into m volume elements and assume that the charge densities in each of them are constant. For simplicity, we take the volume elements with the form of small cylinders, and the radius of each cylinder is taken to be equal to that of the beam envelope at $z_j = (z_{1j} + z_{2j})/2$, where z_{1j} and z_{2j} are the axial coordinates defining the cylinder. We then have

$$\phi_i(\mathbf{r}_i) = \sum_{j=1}^{n} D_{ij}\sigma_j + \sum_{j=n+1}^{n+m} F_{ij}\rho_j, \qquad (i = 1 \ldots n), \tag{83}$$

where D_{ij} is given by Eq. (72) and

$$F_{ij} = \frac{1}{4\pi\varepsilon_0}\int_{V_j}\frac{1}{R_{ij}}dv'. \tag{84}$$

Having in mind the physical interpretation of D_{ij} and F_{ij} we can compute these coefficients by means of the corresponding expressions given in Section III (see also Martínez and Sancho (1988) for details).

2. *Computation of the Trajectories*

The solution to Eq. (83), together with the trajectories in the beam, are obtained by an iterative scheme. This has been done with some approximations in order to simplify the computer program. First, the primary ion source is ignored and the integration starts at a distance h from the third aperture with zero slope; second, a uniform beam density along the radius has been assumed; third, collisions between primary and secondary ions are ignored and the beam is treated as laminar; and finally, the effect of the axial component of the beam is neglected as it is much lower than the one produced by the lens.

As a first step in the iteration, the primary beam profile is determined with all the ρ_k values equal to 0. The resulting beam is divided into small cylinders and a charge density ρ_k is assigned to each, according to the current density and velocity at the point (r_k, z_k). The surface charge densities are then recalculated by means of the expression

$$\sigma_i = \sum_{j=1}^{n}[D^{-1}]_{ij}\left(\phi_j - \sum_{k=n+1}^{n+m} F_{jk}\rho_k\right), \qquad (i = 1 \ldots n), \tag{85}$$

obtained by matrix inversion of Eq. (83). The beam profile is redetermined using the new σ_i and the ρ_k. Several iterative cycles are completed until the beam profile does not change appreciably.

In calculating each new beam profile, we need to know the electric field created by the beam itself. To obtain the radial component of the field, we use Eq. (60). Adding the contribution of the lens we have the total field at each point of the trajectory and then the integration is performed by a central difference formula.

Figure 15 illustrates the results for five values of the perveance; as P increases, the lens is less effective in focusing the primary beam and the repulsion becomes more and more important. The number of required iterations also increases with P from two to five. Figure 16 shows the influence on the the secondary ions. For $P = 10^{-15}$ $(AV^{-3/2})$ the trajectory for a secondary ion, which emerges with an initial energy of 4 eV and parallel to the axis, is very similar to that obtained ignoring space charge. For higher perveances, the lens focusing action is screened and even annulated by the positive beam.

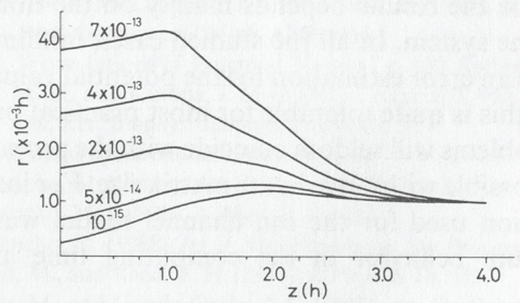

FIG. 15. Profiles of an Ar^+ ion beam for five values of the perveance. The target is located at $z = 0$ and the electrodes at $z/h = 1$, 2, and 3, respectively.

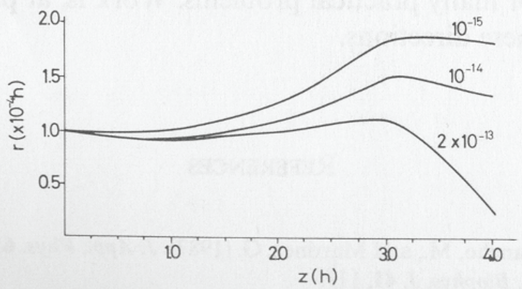

FIG. 16. Trajectories of a secondary negative ion of atomic mass 100 for three values of the perveance of the primary beam.

V. Conclusions

The examples presented in the previous section show clearly that the integral equation method represents a quite advantageous formulation for the majority of electrostatic problems, the exception being those with permittivity varying continuously through the medium. The method has several characteristic advantages: the geometry effective dimension is reduced by one; the potential and field are obtained at any particular point independently from others; and for a given geometry, the matrix coefficients can be obtained once and then used for different conditions of polarization or source distributions.

It has been argued that the integral equation method is awkward to apply because it requires numerical evaluation of complicated integrals appearing in the matrix elements due to the use of nontrivial basis functions. We have shown that these coefficients can be calculated analytically—for systems with rotational symmetry—without loss of accuracy. This can be achieved by taking constant basis functions and making a nonuniform division of the boundaries according to the expected variation of the fields along them.

The accuracy of the results depends mainly on the number of subareas used to simulate the system. In all the studied cases, fulfillment of boundary conditions permits an error estimation for the potential values less than 0.5%. It is believed that this is quite tolerable for most practical purposes, since the actual physical problems will seldom coincide with the proposed models. This high precision is possible with a moderate matrix size. For instance, the matrix maximum dimension used for the ion channel model was 80×80, which implies an optimum behavior in the computing time and memory size required.

Significant developments of the integral equation method are desirable and also expected in the near future. Analysis of systems with not exact rotational symmetry, as the gramicidin channel, could be undertaken by a perturbative technique without introducing an excessive complexity. In the Electron Optics field, the introduction of nonuniform space charge beams would be useful for many practical problems. Work is, at present, being carried out in both these directions.

References

Algora del Valle, C., Sancho, M., and Martínez, G. (1987). *J. Appl. Phys.* **61**, 4571.

Andersen, O. S. (1983). *Biophys. J.* **41**, 119.

Andersen, O. S., Koeppe, R. E. II, Durkin, J. T., and Mazet, J. L. (1987). *In* "Ion transport through membranes," p. 295. Academic Press, New York.

Byrd, P. F., and Friedman, M. D. (1971). "Handbook of Elliptic integrals for Engineers and Scientists." Springer-Verlag, Berlin.

Chutjian, A. (1979). *Rev. Sci. Instrum.* **7**, 981.

Daumas, P., Heitz, F., Ranjalahy-Rasoloarijao, L., and Lazaro, R. (1989). *Biochimie* **71**, 77.

Durand, E. (1964). "Electrostatique I." Masson, Paris.

Frömter, E. (1983). *In* "Biophysics." (W. Hoppe, W. Lohmann, H. Markl and H. Ziegler, eds.), p. 465. Springer-Verlag, Berlin and New York.

Gerald, C. (1984). "Applied Numerical Analysis." Addison-Wesley, Massachusetts.

Gradshteyn, I. S., and Ryzhik, I. M. (1980). "Tables of Integrals, Series and Products." Academic Press, New York.

Grivet, P. (1972). "Electron Optics." Pergamon Press, Oxford.

Harrington, R. F. (1968). "Field Computation by Moment Methods." Macmillan, New York.

Harting, E., and Read, F. H. (1976). "Electrostatic Lenses." Elsevier, Amsterdam.

Hawkes, P. W. (1987). *Nucl. Instrum. and Meth.* **A258**, 462.

Heddle, D. W. O. (1971). *J. Phys. E* **7**, 981.

Heddle, D. W. O., and Kurepa, M. V. (1970). *J. Phys. E* **3**, 552.

Jackson, J. D. (1980). "Electrodinámica Clásica," p. 76. Alhambra, Madrid.

Jordan, P. C. (1982). *Biophys. J.* **39**, 157.

Jordan, P. C. (1986). *In* "Ion Channel Reconstitution." (C. Miller, ed.), p. 37. Plenum Press, New York.

Jordan, P. C. (1989). Private communication.

Jordan, P. C., Bacquet, R. J., McCammon, J. A., and Tran, P. (1989). *Biophys. J.* **55**, 1041.

Kasper, E. K. (1987). *Nucl. Instrum. and Meth.* **A258**, 466.

Kellog, O. D. (1967). "Foundations of Potential Theory," p. 160. Springer-Verlag, Berlin.

Kurepa, H. V., Tasic M. D., and Kurepa, J. M. (1974). *J. Phys. E* **7**, 940.

Levitt, D. G. (1986). *Ann. Rev. Biophys. Biophys. Chem.* **15**, 29.

Liebl, H. (1983). *Int. J. Mass Spectrom. Ion Phys.* **46**, 511.

Martínez, G., and Sancho, M. (1983a). *Am. J. Phys.* **51**, 170.

Martínez, G., and Sancho, M. (1983b). *J. Phys. E.* **16**, 625.

Martínez, G., and Sancho, M. (1988). *Int. J. Mass Spectrom. Ion Processes* **84**, 221.

Martínez, G., Sancho, M., and Read, F. H. (1983). *J. Phys. E* **16**, 631.

Martínez, G., Sancho, M., and García-Galán, J. C. (1987). *An. Fis. Ser. B* **83**, 225.

Munro, E. (1987). *Nucl. Instrum. and Meth.* **A258**, 443.

Parsegian, V. A. (1969). *Nature* **221**, 844.

Parsegian, V. A. (1975). *Ann. N. Y. Acad. Sci.* **264**, 161.

Renau, A., Read, F. H., and Brunt, J. N. (1982). *J. Phys. E* **15**, 347.

Steele, C. W. (1987). "Numerical Computation of Electric and Magnetic Fields." Van Nostrand Reinhold, New York.